Excellent piezoelectric property and thermal stability of Pb(Sc, Nb)O3-Pb(Hf, Ti)O3 ceramic

Mo Zhao (zhaomoxjtu@163.com)
Xi'an Jiaotong University https://orcid.org/0000-0002-7164-0713
Li Jin
Xi'an Jiaotong University
Wei Chen
Northwest Institute of Nuclear Technology
Wei Wu
Northwest Institute of Nuclear Technology

Research Article

Keywords: Pb(Sc, Nb)O3-Pb(Hf, Ti)O3 ceramic, piezoelectric property, thermal stability

Posted Date: April 6th, 2021

DOI: https://doi.org/10.21203/rs.3.rs-242676/v1

Abstract

xPb(Sc 1/2 Nb 1/2)O 3 -(1-x)Pb(Hf 1-y Ti y)O 3 piezoelectric ceramics were prepared by solid state route, and the phase structures and piezoelectric properties of ceramics were systematically investigated. Results showed that the sample with the composition of x=0.07 and y=0.53 possessed higher phase coexistence between the rhombohedral and tetragonal, and exhibited the optimal properties among different constituent systems, i.e. T C =355 °C, d 33 =400 pC/N, ε r =1390 and tan δ =1.05%. Furthermore, the effects of temperature on d 33 , leakage current density, P - E loop, and unipolar strain were studied for xPb(Sc 1/2 Nb 1/2)O 3 -(1-x)Pb(Hf 0.47 Ti 0.53)O 3 samples. The sample with x=0.07 revealed better temperature stability as well, the reason of which was analyzed in detail. The study indicates that the 0.07Pb(Sc 1/2 Nb 1/2)O 3 -0.93Pb(Hf 0.47 Ti 0.53)O 3 piezoelectric ceramic has excellently comprehensive properties suitable for application in higher temperature condition.

1. Introduction

Piezoelectric materials are typical materials that enable to realize the invertible conversion between mechanical energy and electrical energy. Until now, lead-based piezoelectric ceramics have gotten wide applications in many fields, e. g., sensors, actuators, and filters sensors [1-3]. Recently, relaxor ferroelectrics have been extensively investigated due to their high piezoelectric properties, including $Pb(Ni_{1/3}Nb_{2/3})O_3$-$Pb(Zr,Ti)O_3$(PNN-PZT), $Pb(Sb_{1/2}Nb_{1/2})O_3$-$PbTiO_3$ (PSN-PT), $Pb(Mg_{1/3}Nb_{2/3})O_3$-$PbTiO_3$ (PMN-PT), and $Pb(Zn_{1/3}Nb_{1/3})O_3$-$Pb(Zr,Ti)O_3$ (PZN-PZT), etc [4-9]. For example, Li et al. [10] reported the ultrahigh piezoelectric coefficient (d_{33}=1500 pC/N) for Sm-doped $Pb(Mg_{1/3}Nb_{2/3})O_3$-$PbTiO_3$ (PMN-PT) ceramic. However, high piezoelectric coefficient inevitably gives rise to the decline of Curie temperature T_C [11]. Among relaxor ferroelectrics, $Pb(Me,Nb)O_3$-$Pb(Zr,Ti)O_3$ (Me=Sc^{3+}, In^{3+}, or Yb^{3+}) systems exhibit better comprehensive character in d_{33} and T_C. Zheng et al. [12] prepared Pb(Yb,Nb)-$Pb(Zr,Ti)O_3$ ceramics with d_{33}=268 pC/N and T_C=392.2 °C. Furthermore, Zhu et al. [13] found higher properties of $Pb(Sc, Nb)O_3$-$Pb(Zr, Ti)O_3$ ceramic, with d_{33}= 449 pC/N and T_C=322 °C.

However, with the progress of science and technology, higher requirements are put forward for piezoelectric devices. The high-temperature failure of piezoelectric materials has become a major problem that plagues the development of piezoelectric devices. A ceramic system with high Curie temperature and excellent piezoelectric performance must be selected to ensure that piezoelectric devices can work normally in a wide temperature range. Therefore, the development of high Curie temperature piezoelectric ceramic materials with excellent performance has become an urgent task.

It has been proved that the phase diagram of $PbHfO_3$-$PbTiO_3$ (PHT) is similar to that of PZT [14, 15]. When PT content is about 50%, tetragonal and rhombohedral phases are coexistent. The T_c of PHT could reach to 340°C. In addition, it was found that the introduction of PHT into relaxor ferroelectrics could significantly improve piezoelectric and dielectric properties. Wang et al. found that the d_{33} (680 pC/N) and T_c (276 ℃) of ternary $Pb(Mg,Nb)O_3$-PHT ceramic are higher than that of $Pb(Mg,Nb)O_3$-PZT ceramic

[16]. And Yan et al. reported the ternary system $Pb(Ni,Nb)O_3$-PHT ceramic with d_{33}=950 pC/N [17]. Therefore, the introduction of PHT constituent into system is expected to exhibit higher values of T_C and d_{33}. It can be made to have better performance by compounding with other lead-based solid solutions, optimizing the preparation process, adjusting the composition to the morphotropic phase boundary (MPB), and further doping modification.

In this study, the $Pb(Sc_{1/2}Nb_{1/2})O_3$-$Pb(Hf_{0.47}Ti_{0.53})O_3$ (PSN-PHT) ceramics were prepared by conventional solid phase route. The phase structure and piezoelectric, ferroelectric, and dielectric properties of PSN-PHT ceramics were investigated in detail. The thermal stability of as-prepared samples was discussed.

2. Experimental

The material system was $xPb(Sc_{1/2}Nb_{1/2})O_3$-$(1-x)Pb(Hf_{1-y}Ti_y)O_3$, with x value range from 0.06 to 0.22 and y from 0.53 to 0.60. $ScNbO_4$ was firstly synthesized from high purity scandium oxide (99.9%) and niobium oxide (99.9%) at 1050 ^oC for 6h. Then, Pb_3O_4 (99.9%), as-prepared ScNbO4, TiO2 (99.9%), and HfO_2 (99.99%) were stoichiometrically weighed and milled for 15 h. The batches were calcined for 4 h at 900 °C, and the synthesized powers were shaped to form disks with the diameter of 12 mm at a pressure of 200 MPa. Finally, the disks were immersed in lead tetroxide powder and sintered for 2 h at 1200-1250 °C in a covered alumina crucible to prepare ceramics. For electrical property measurement, Ag paste was sintered on both sides of polished ceramic samples. Electric poling was carried out by applying a 20 kV/cm field at 150 °C.

The crystalline phases of samples were determined by X-ray diffraction (XRD, Bruker D8 Advance) with CuKα radiation. The morphologies were observed by scanning electron microscopy (SEM, JEOL JSM 6700F). The piezoelectric coefficient d_{33} was measured using a piezo-d_{33} meter (ZJ-3A, Chinese Academy of Science). The temperature dependence of relative dielectric permittivity was carried out by impedance analyzer (E4990A, Agilent, Palo Alto, CA, US) in the temperature range of 25-450 °C. Ferroelectric hysteresis loop and unipolar strain were performed by ferroelectric test system (aix ACCT TF3000, Aachen, Germany) at 0.05 Hz. The temperature dependence of leakage current for PSN-PHT sample was measured by leakage current tester (Test NS200T, CN).

3. Results And Discussion

Fig. 1 shows the density of PSN-PHT ceramics as a function of the PSN content for different sintering temperatures. It can be seen that the bulk density of samples increases with increasing sintering temperature up to 1250 ^oC. Further increasing the sintering temperature above 1250 ^oC even causes a decrease. So 1250^oC appears to be the most suitable sintering temperature. The XRD patterns of $xPb(Sc_{1/2}Nb_{1/2})O_3$-$(1-x)Pb(Hf_{0.47}Ti_{0.53})O_3$ samples with different PSN contents are shown in Fig. 2. Results show that a single perovskite phase appears for all the samples, without any impurity phase. The two spliting peaks located at 2θ=45° indicate there contains the tetragonal phase in perovskite structure

[18, 19]. Additionally, with the increase in PSN content, one can see that the intensities of two splitting peaks change obviously, reflecting the discrepancy in phase composition.

In order to determine the change of tetragonal phase proportion in perovskite structure, the peaks at 2θ = 45° were slowly scanned corresponding to (200) crystal plane and the fitting curves are shown in Fig. 3 (a)-(d) [20, 21]. As can be seen, there have rhombohedral and tetragonal phases in all the samples. The tetragonal phases are marked by $(200)_T$ and $(002)_T$, while the rhombohedral phase by $(020)_R$. Here, the volume fraction of tetragonal phase could be estimated according to Eq. (1) [22]:

$$\varphi = \frac{I_T}{I_R + I_T} = \frac{I(002)_T + I(200)_T}{I(020)_R + I(200)_T + I(002)_T} \quad (1)$$

Where φ represents the tetragonal volume fraction, I_T represents diffraction intensities of (002) and (200) phases, and I_R represents the diffraction intensity of (020) peak. Fig. 3(e) shows the variation of tetragonal phase fraction with PSN content. Initially, the tetragonal fraction decreases with increasing PSN content, which is attributed to the increase in diffraction peak intensity of rhombohedral phase. When x = 0.07, the tetragonal fraction decreases to 83%, indicating that the degree of phase coexistence between the tetragonal and rhombohedral is higher. This also illustrates that the $0.07Pb(Sc_{1/2}Nb_{1/2})O_3$-$0.93Pb(Hf_{0.47}Ti_{0.53})O_3$ sample locates at morphotropic phase boundary (MPB) region.

Fig. 4(a) shows the d_{33} for PSN-PHT piezoelectric ceramics sintered at 1200 and 1250 °C. As a whole, the d_{33} of ceramics sintered at 1250°C is higher than that of samples at 1200°C, and all the d_{33} increases firstly, and then decreases with increasing PSN content. In this study, for y=0.53, a higher d_{33} of 400 pC/N was achieved for the sample with x=0.07 and y=0.53. Figure 4(b) shows the temperature dependence of both the relative dielectric permittivity and the dielectric loss of $xPb(Sc_{1/2}Nb_{1/2})O_3$-$(1-x)Pb(Hf_{0.47}Ti_{0.53})O_3$ piezoelectric ceramics at a frequency of 1 kHz. It can be seen that with the increase of temperature, the relative dielectric permittivity and dielectric loss of PSN-PHT piezoelectric ceramics have increased significantly at the beginning. With the further increase in temperature, when the temperature exceeds the Curie temperature, the piezoelectric ceramic will undergo a transition from the ferroelectric phase to the paraelectric phase. Both the relative dielectric permittivity and the dielectric loss decrease rapidly. Table 1 shows the electrical parameters of $xPb(Sc_{1/2}Nb_{1/2})O_3$-(1-x) $Pb(Hf_{0.47}Ti_{0.53})O_3$ samples. It is obvious that the T_c (Curie temperature) changes slightly with the increase of PSN content. In the case of x=0.06, T_c value is the maximum, about 359°C, while the T_c for x=0.07 is the minimum, about 355 °C. The loss tangent (tanδ) at room temperature almost keeps constant at lower PSN content, and slightly increases when x =0.09. Notably, the relative dielectric permittivity ε_r exhibits opposite trend compared to tanδ. The ε_r eventually increases, with the maximum value of 1424 for x= 0.08. It can be seen from the table 1 that when x =0.07, y =0.53, the sample achieves the optimal performance, i.e. T_C=355 °C, d_{33}=400 pC/N, e_r=1390 and tan$d$ =1.05%, arising from phase coexistence between the rhombohedral and tetragonal in perovskite structure. In the MPB region, the rhombohedral phase and the tetragonal phase coexist. As we

all know that there are 8 possible polarization directions for rhombohedral phase and 6 for tetragonal phase. There are 14 possible spontaneous polarization directions at the phase boundary where two phases coexist. During the poling process, the orientation of domain is easier to follow the direction of external electric field: this process confers excellent dielectric and piezoelectric properties to the specimens. According to the thermodynamic analysis, the energy difference from phases for material is extremely low in the region of MPB, and the distribution of thermodynamic energy is relatively balanced, which results in lower domain wall energy and smaller ferroelectric domain. This is beneficial to the domain wall motion and the improvement of piezoelectric properties. In addition, as shown in Fig. 4, no other dielectric peaks are observed in the temperature range from 25 °C to 450 °C. which indicates that there is only the phase transition from the ferroelectric to paraelectric [23].

Table 1 Electrical parameters of $xPb(Sc_{1/2}Nb_{1/2})O_3$-(1-x) $Pb(Hf_{0.47}Ti_{0.53})O_3$ samples.

Sample	ε_r	d_{33}(pC/N)	tanδ (%)	T_c(°C)
x=0.06	1128	225	1.08	359
x=0.07	1390	400	1.05	355
x=0.08	1424	360	1.06	356
x=0.09	1209	355	1.12	358

Fig. 5 compares the Curie temperature and piezoelectric constant of the PSN-PHT ceramics prepared in this study with other lead-based ceramics and lead-free ceramics. It can be found that although many lead-based ceramics have good piezoelectric properties, the Curie temperature is relatively low. Lead-free piezoelectric ceramics have a high Curie temperature but weak piezoelectric response. The optimal performance of $Pb(Sc_{1/2}Nb_{1/2})O_3$-$Pb(Hf_{0.47}Ti_{0.53})O_3$, which reached 400 pC/N with a high Curie temperature of 355°C, could improve the shortcomings of the above system and has important advantages in practical applications. The results show that PSN-PHT ceramics are beneficial to the development of high temperature piezoelectric devices.

Fig. 6(a) shows the hysteresis loops for xPSN-PHT ceramics. All the samples display typical ferroelectric hysteresis loops, and the hysteresis loops are nearly saturated at the electrical field of 30kV/cm. Fig. 6(b) depicts the variation of remnant polarization (P_r) with PSN content. As can be seen, the P_r reaches to a maximum value of 18μC/cm^2 at x=0.07. It ascribes mainly as the fact that the sample constituent may be located at MPB region. In the MPB region, the energy difference from phases is extremely low, and the distribution of thermodynamic energy is relatively balanced, which results in lower domain wall energy and smaller ferroelectric domain. These are positive to improve the domain wall motion and increase P_r [30, 31]. The intrinsic component of d_{33} in perovskite ferroelectrics could be described by Eq. (2).

$$d_{33} = 2P_s\varepsilon_{33}Q_{33} \qquad (2)$$

Where P_s denotes the spontaneous polarization, Q_{33} denotes the electrostrictive coefficients and ε_{33} denotes the relative dielectric permittivity [32]. Accordingly, the variation trend of d_{33} with PSN content is consistent with that of P_r. The improvement of d_{33} could be achieved by the increase of P_r.

Fig. 7(a) shows the uniploar strains of xPSN-PHT ceramics sintered at 1250°C. According to the slope of the unipolar *S*-*E* curve for the sample with x=0.07, the maximum inverse piezoelectric coefficient d_{33}^* of 536 pm/V was obtained, as shown in Fig. 7(b). Here, the change trend of d_{33}^* is similar to the d_{33} with PSN content, but the value of d_{33}^* is greater than that of d_{33}. In general, the measurement method on inverse piezoelectric coefficient makes the sample more sufficient polarized than quasi-static method. On the other hand, the d_{33}^* is dominated by the intrinsic (lattice) and reversible internal interface motion (the extrinsic piezoelectric contributions) [33]. The extrinsic contribution is attributed mainly to the movement of non-180° domain walls. The d_{33} is only derived from the intrinsic piezoelectric response. The presence of 109°/71° domain walls and 90° domain walls have been confirmed in the rhombohedral and tetragonal phases [34], which are responsible for the larger value of d_{33}^*.

The operating temperature of electronic devices is often about 75-150°C, So it is of great significance to investigate the thermal stability of piezoelectric ceramic. Fig. 8(a) shows the temperature stability profiles of d_{33} for xPSN-PHT ceramics after heating treatment at different temperatures. All the d_{33} do not have obvious change below 150°C. For the sample with x=0.07, the value of d_{33} decreases by only 1.2% at the depoling temperature of 150 °C. When the temperature increases to 250°C, the decline in d_{33} is still less than 10%. If the temperature is further raised to 300 °C, the decrease in d_{33} is only about 15%. Therefore, The sample with x=0.07 shows a good thermal stability at the temperature below 300 °C. When the depoling temperature is above 300 °C, the d_{33} of all the samples sharply declines. If the content of PSN is further increased, the thermal stability of the ceramics will decrease. It is possibly due to larger variation in tolerance factor of the sample with the increasing PSN content, which would give rise to large lattice distortion, thus reducing thermal stability.

The tolerance factor *t* can be calculated by the following formula:

$$t = \frac{R_A + R_O}{\sqrt{2}\left(R_B + R_O\right)} \quad (3)$$

In the formula, r_A, r_B, and r_O are the radius of A, B and O ions, respectively. It can be seen from table 2 that with the increasing PSN content, the deviation of tolerance factor from “1” increases, which indicates that the structural distortion becomes larger, thus reducing the thermal stability [35].

Table 2 The calculated tolerance factor for PSN-PHT ceramics

PSN content	average radius at B site (Å)	t
0.06	0.6563	0.9938
0.07	0.6567	0.9936
0.08	0.6571	0.9934
0.09	0.6575	0.9932

Fig. 8(b) shows the change in the thermal stability of leakage current density for xPSN-PHT samples, which were measured at 30 kV/cm in the temperature range of 40-200 °C. With increasing temperature, the leakage current density does not change significantly at first. However, it increases rapidly at the temperature higher than 160 °C. The leakage current density for the sample with x=0.06 is about 5.2×10^{-6} A/cm^2 at 200 °C, higher than the sample with x=0.07 (3.98×10^{-6}A/cm^2). It is known that larger leakage current would cause the increase of heat and loss during repeated operation, thereby deteriorating the performance [23]. Here, the sample with x=0.07 exhibits higher thermal stability.

The temperature character of 0.07PSN-PHT sample was investigated according to *P–E* hysteresis loops as depicted in the Fig. 9(a). Similarly, the remnant polarization (P_r) does not obviously change at first with increasing temperature, which increases rapidly as the temperature is above 120 °C. The remnant polarization increases from 17.7 mC/cm^2 at 25 °C to 24.4 mC/cm^2 at 130 °C. This phenomenon had been proved in perovskite ferroelectrics [36]. It is due possibly to the enhancement of thermodynamic activity with the increase of temperature, which makes the domain reverse readily, leading to the increase of P_r. However, when the temperature is higher than 150 °C, the *P-E* curve becomes distorted due to the sharp increase in leakage current density.

From the perspective of application, the thermal stability of unipolar strain is of great significance for actuators and sensors. Fig. 10(a) shows the temperature behavior of unipolar strain for 0.07PSN-PHT sample, and the strain as a function of temperature is presented in Fig. 10(b). As indicated in Fig. 10(b), the strain gradually increases with the temperature. The value of strain increases from 1.63% at room temperature to 1.97% at 130 °C, which is beneficial to high temperature application. At high temperature, the thermal energy of domain and the activation energy of domain wall decrease, and the domains are easy to turn over, contributing to the increase of strain.

4. Conclusions

$xPb(Sc_{1/2}Nb_{1/2})O_3$-(1-x)$Pb(Hf_{1-y}Ti_y)O_3$ ternary piezoelectric ceramics were prepared by conventional solid state route. For x=0.07 and y=0.53, the sample exhibited excellent piezoelectric properties, i.e. T_C=355 °C, d_{33}=400 pC/N, e_r=1390 and tan$d$ =1.05%, arising from phase coexistence between the rhombohedral and tetragonal in perovskite structure. Meanwhile, the thermal stability of $xPb(Sc_{1/2}Nb_{1/2})O_3$-(1-x) $Pb(Hf_{0.47}Ti_{0.53})O_3$ samples was analyzed. Results showed that the sample with x=0.07 had good thermal

stability in piezoelectric coefficient d_{33}, leakage current density, *P-E* loop, and unipolar strain, illustrating the tailored role of constituent. The excellent properties of $Pb(Sc_{1/2}Nb_{1/2})O_3$-$Pb(Hf_{0.47}Ti_{0.53})O_3$ piezoelectric ceramic indicate its promising application in the environment at higher temperature.

Declarations

Funding: Not applicable.

Conflicts of interest/Competing interests: There are no competing financial interestsor personal relationships that could have appeared to influence the work reported in this paper.

Availability of data and material: Not applicable.

Code availability: Not applicable.

References

[1] S.E. Park, T.R. Shrout, Ultrahigh strain and piezoelectric behaviour in relaxor based ferroelectric single crystals, J. Appl. Phys. 82 (1997) 1804–1811.

[2] R.C. Turner, P.A. Fuierer, R.E. Newnham, T.R. Shrout, Materials for high temperature acoustic and vibration sensors: A review, Appl. Acoust. 41 (1994) 299–324.

[3] S. Zhang, F. Yu, Piezoelectric materials for high temperature sensors, J. Am. Ceram. Soc. 94 (2011) 3153–3170.

[4] I. Grinberg, M.R. Suchomel, P.K. Davies, A.M. Rappe, Predicting morphotropic phase boundary locations and transition temperatures in Pb and Bi-based perovskite solid solutions from crystal chemical data and first-principles calculations, J. Appl. Phys. 98 (2005) 094111.

[5] B. Praveenkumar, H.H. Kumar, D.K. Kharat, B.S. Murty, Investigation and characterization of La-doped PZT nano crystalline ceramics prepared by mechanical activation route, Mater. Chem. Phys. 112 (2008) 31–34.

[6] A. Hall, M. Allahverdi, E.K. Akdogan, A. Safari, Piezoelectric/electrostrictive multi material PMN-PT monomorph actuators, J. Eur. Ceram. Soc. 25 (2005) 2991–2997.

[7] H. Uršič, B. Malič, J. Cilenšek, T. Rojac, B. Kmet, M. Kosec, Linear thermal expansion coefficients of relaxor-ferroelectric $0.57Pb(Sc_{1/2}Nb_{1/2})O_3–0.43PbTiO_3$ ceramics in a wide temperature range, J. Eur. Ceram. Soc. 33 (2013) 2167–2171.

[8] X.Y. Gao, J.E. Wu, Y. Yu, Z.Q. Chu, H.D. Shi, S.X. Dong, Giant piezoelectric coefficients in relaxor piezoelectric ceramic PNN-PZT for vibration energy harvesting, Adv. Fun. Mater. 28 (2018) 1706895.

[9] M. Kobune, K. Muto, Y. Akiyama, Piezoelectric and ferroelectric properties of $Pb(Zn_{1/3}Nb_{2/3})O_3$-$PbTiO_3$-$PbZrO_3$ ceramics, J. Ceram. Soc. Jpn. 110 (2002) 12–17.

[10] F. Li, D. Lin, Z. Chen, Z. Cheng, J. Wang, C. Li, Z. Xu, Q. Huang, X. Liao, L.Q. Chen, T.R. Shrout, S. Zhang, Ultrahigh piezoelectricity in ferroelectric ceramics by design, Nat. Mater. 17 (2018) 349–354.

[11] S. Zhang, L.C. Lim, Complete sets of elastic, dielectric, and piezoelectric properties of [001]-poled Rhombohedral $Pb(Zn_{1/3}Nb_{2/3})O_3$-(4.5-7)%$PbTiO_3$ single crystals, IEEE T. Ultrason. Ferr. 66 (2019) 816–819.

[12] Y. Zhang, H. Chen, D. Mao, Processing, structure, and electrical properties of MnO_2-doped $Pb(Yb_{1/2}Nb_{1/2})(0.10)(Zr_{0.47}Ti_{0.53})(0.90)O_3$ ceramics Ceram. Int. 39 (2013) S159–S163.

[13] Z. Zhuo, Z. Ling, Y. Liu, Phase composition and piezoelectric properties of $Pb(Sb_{1/2}Nb_{1/2})$–$PbTiO_3$–$PbZrO_3$ ceramics, J. Mater. Sci-Mater. El. 29 (2018) 9524–9530.

[14] M.A.D.L. Rubia, R.E. Alonso, J.D. Frutos, A.R. López-Garcia, Phase transitions in $PbTi_xHf_{1-x}O_3$ determined by thermal analysis and impedance spectroscopy, IEEE. Tultrason. Ferr. 98 (2009) 793–799.

[15] G. Fantozzi, H. Idrissi, C. Favotto, M. Roubin, Lead hafnate titanate (PHT) ceramics: processing and properties, J. Eur. Ceram. Soc. 20 (2000) 1671–1676.

[16] D. Wang, M. Cao, S. Zhang, J.L. Jones, Investigation of ternary system $PbHfO_3$-$PbTiO_3$-$Pb(Mg_{1/3}Nb_{2/3})O_3$ with morphotropic phase boundary compositions, J. Am. Ceram. Soc. 95 (2012) 3220–3228.

[17] Y. Yan, Z. Li, Y. Xia, M. Zhao, M. Zhang, D. Zhang, Ultra-high piezoelectric and dielectric properties of low-temperature sintered lead hafnium titanate-lead niobium nickelate ceramics, Ceram, Int. 46 (2020) 5448–5453.

[18] N. Luo, S. Zhang, Q. Li, C. Xu, Z. Yang, Q. Yan, Y. Zhang, T.R. Shrout, New $Pb(Mg_{1/3}Nb_{2/3})O_3$-$Pb(In_{1/2}Nb_{1/2})O_3$-$PbZrO_3$-$PbTiO_3$ quaternary ceramics: morphotropic phase boundary design and electrical properties, ACS. Appl. Mater. Inter. 8 (2016) 15506–15517.

[19] Y. Yan, Z. Li , M. Zhang, P. Sun, Y. Xu, Y. Feng, Effect of Fe substitution on the piezoelectric, dielectric and ferroelectric properties of PNZST ceramics , Ceram. Int. 42 (2016) 18352–18356.

[20] G. Cilaveni, K.V.A. Kumar, S.S.K. Raavi, C. Subrahmanyam, S. Asthana, Control over relaxor, piezo-photocatalytic and energy storage properties in $Na_{0.5}Bi_{0.5}TiO_3$ via processing methodologies, J. Alloy. Compd. 798 (2019) 540–552.

[21] M. Makaremi, M.S. Jhon, M.S. Mauter, L.T. Biegler, Surface wetting study via pseudocontinuum modeling, J. Phys. Chem. C. 120 (2016) 11528–11534.

[22] C. Bedoya, C.H. Muller, A. Kowalski, E. Nigrelli, Investigation of the morphotropic region in the Sr-doped lead Hafnate-Titanate solid solution $Pb_{0.94}Sr_{0.06}Hf_{1-x}Ti_xO_3$, J. Mater. Sci. Mater. El. 12 (2001) 543-550.

[23] B. Deng, Q. Wei, C. He, Z. Wang, X. Yang, X. Long, Effect of $Pb(Mn_{1/3}Sb_{2/3})O_3$ addition on the electrical properties of $BiScO_3$-$PbTiO_3$ piezoelectric ceramics, J. Alloy. Comp. 790 (2019) 397–404.

[24] D. Wang, M. Cao, S. Zhang, Investigation of ternary system $PbHfO_3$-$PbTiO_3$-$Pb(Mg_{1/3}Nb_{2/3})O_3$ with morphotropic phase boundary compositions, J. Am. Ceram. Soc. 95 (2012) 3220–3228.

[25] P. Li, J. Zhai, B. Shen, S. Zhang, X. Li, F. Zhu, X. Zhang, Ultrahigh piezoelectric properties in textured (K,Na)NbO_3-Based lead-free ceramics, Adv. Math. 30 (2018) 1705171–1705179.

[26] R. Zhu, W. Ji, B. Fang, D. Wu, Z. Chen, J. Ding, X. Zhao, H. Luo, Ferroelectric phase transition and electrical conduction mechanisms in high Curie-temperature PMN-PHT piezoelectric ceramics, Ceram. Int. 43 (2017) 6417–6424.

[27] D. Pang, X. Long, H. Tailor, A lead-reduced ferroelectric solid solution with high curie temperature: $BiScO_3$-$Pb(Zn_{1/3}Nb_{2/3})O_3$-$PbTiO_3$, Ceram. Int. 40 (2014) 12953–12959.

[28] J. Zheng, Z. Chen, B. Fang, J. Ding, X. Zhao, H. Xu, H. Luo, Synthesis and characterization of $Pb(Yb_{1/2}Nb_{1/2})O_3$-based high-Curie temperature piezoelectric ceramics, Eur. Phys. J. Appl. Phys. 66 (2014) 30101.

[29] F. Gao, H. Rongzi, L. Jiaji, L. Zhen, C. Lihong, T. Changsheng, Phase structure and piezoelectric properties of high Curie temperature $BiYbO_3$-$PbTiO_3$-$BaTiO_3$ ceramics, J. Alloys. Compd. 475 (2009) 619–623.

[30] D. Damjanovic, Commments on origins of enhanced piezoelectric properties in ferroelectrics. IEEE T. Ultrason. Ferr. 56 (2009) 1574–1585.

[31] H. Fu, R.E. Cohen, Polarization rotation mechanism for ultrahigh electromechanical response in single-crystal piezoelectrics, Nature. 403 (2000) 281–283.

[32] Y. Yan, Y. Xu, Y. Feng, Effect of Mn doping on the piezoelectric properties of $0.82Pb(Zr_{1/2}Ti_{1/2})O_3$–$0.03Pb(Mn_{1/3}Sb_{2/3})O_3$–$0.15Pb(Zn_{1/3}Nb_{2/3})O_3$ ferroelectric ceramics, Ceram. Int. 40 (2014) 5897–5903.

[33] Y. Yan, Z. Liu, Z. Li, M. Zhang, D. Zhang, Y. Feng, Improving piezoelectric properties of $Pb(Ni, Nb)O_3$-$Pb(Hf, Ti)O_3$ ceramics by LiF addition, Ceram. Int. 44 (2018) 5790–5793.

[34] F. Barzegar, D. Damjanovic, N. Setter, The effect of boundary conditions and sample aspect ratio on apparent piezoelectric coefficient determined by direct quasistatic method, IEEE T. Ultrason. Ferr. 51 (2004) 262–270.

[35] E. Hou, Y. Yan, M. Zhang, D. Zhang, Z. Li, Morphotropic region and piezoelectric properties of $xPb(In_{1/2}Nb_{1/2})O_3$-(1-x)$Pb(Hf_{1-y}Ti_y)O_3$ ceramics, Ceram. Int. 17 (2020) 27394–27400.

[36] A. Sehirlioglu, A. Sayir, F. Dynys, High temperature properties of $BiScO_3$–$PbTiO_3$ piezoelectric ceramics, J. Appl. Phys. 106 (2009) 014102.

Figures

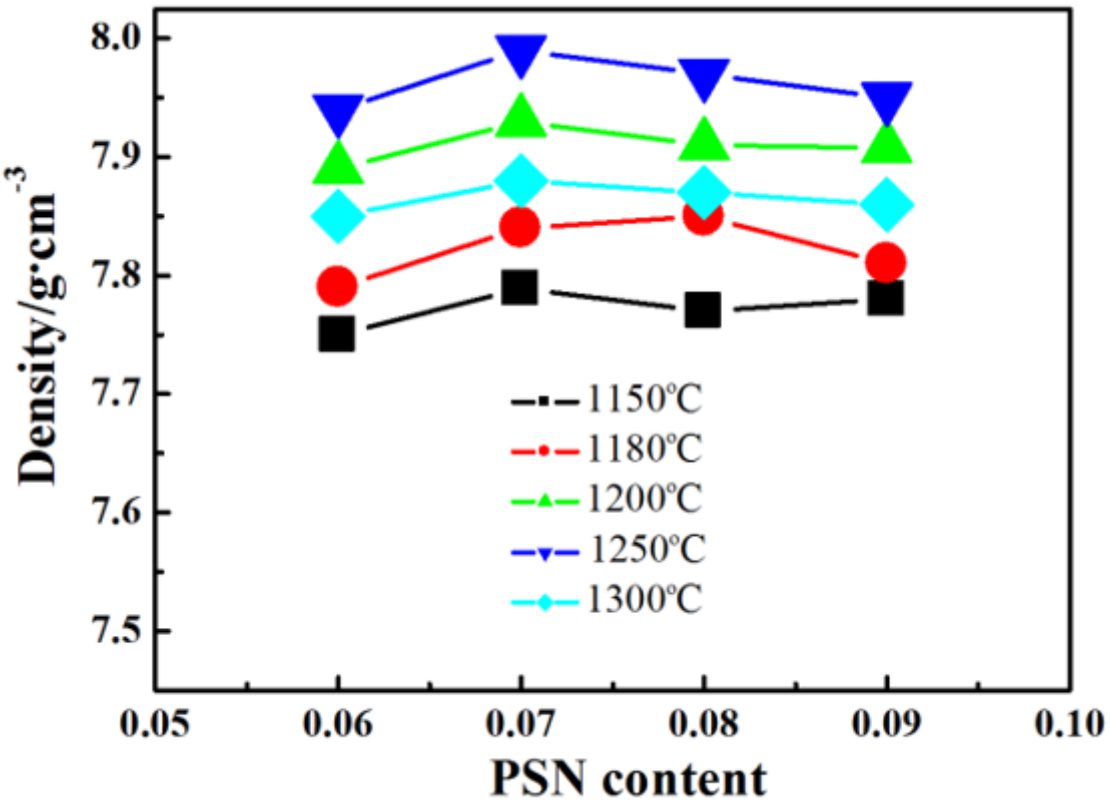

Figure 1

The density of xPb(Sc1/2Nb1/2)O3-(1-x)Pb(Hf0.47Ti0.53)O3 ceramics as a function of the PSN content for different sintering temperatures.

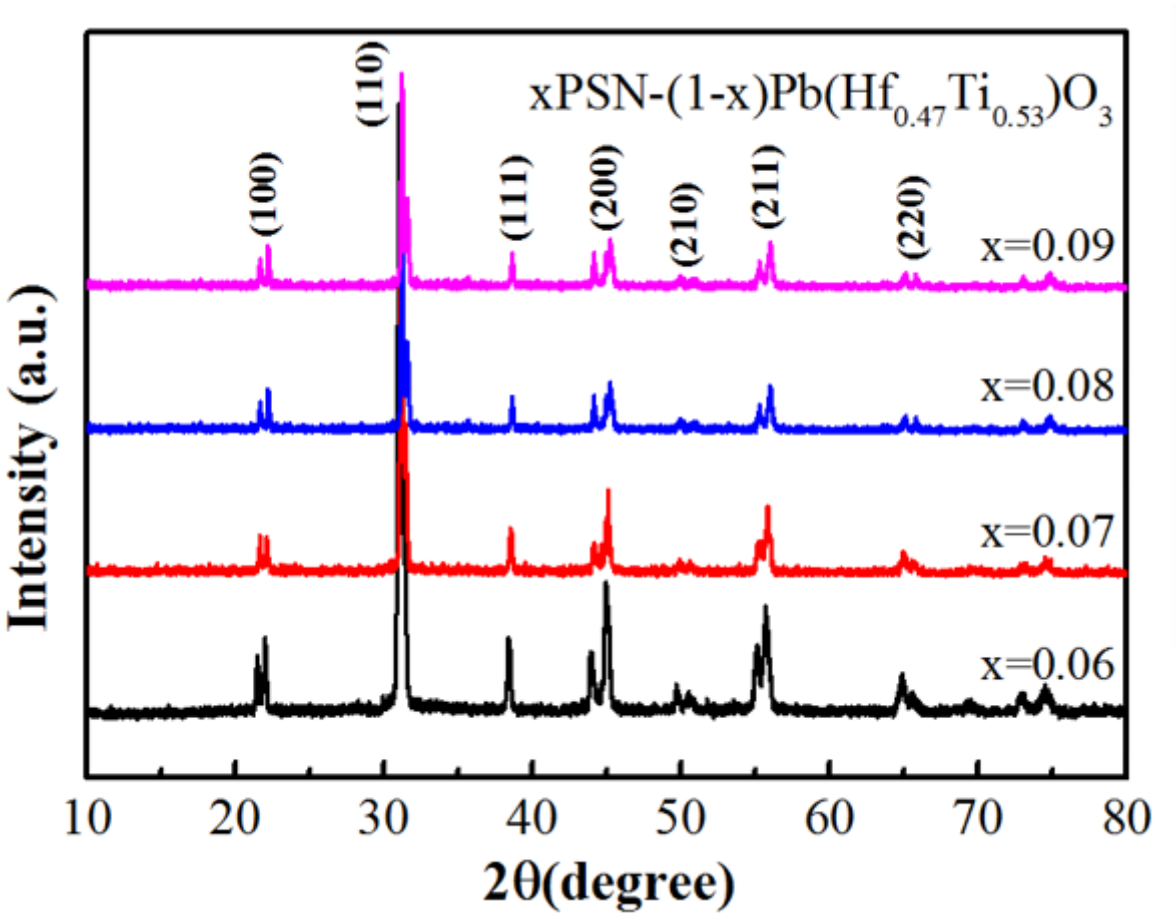

Figure 2

XRD patterns of xPb(Sc1/2Nb1/2)O3-(1-x)Pb(Hf0.47Ti0.53)O3 ceramics sintered at 1250°C.

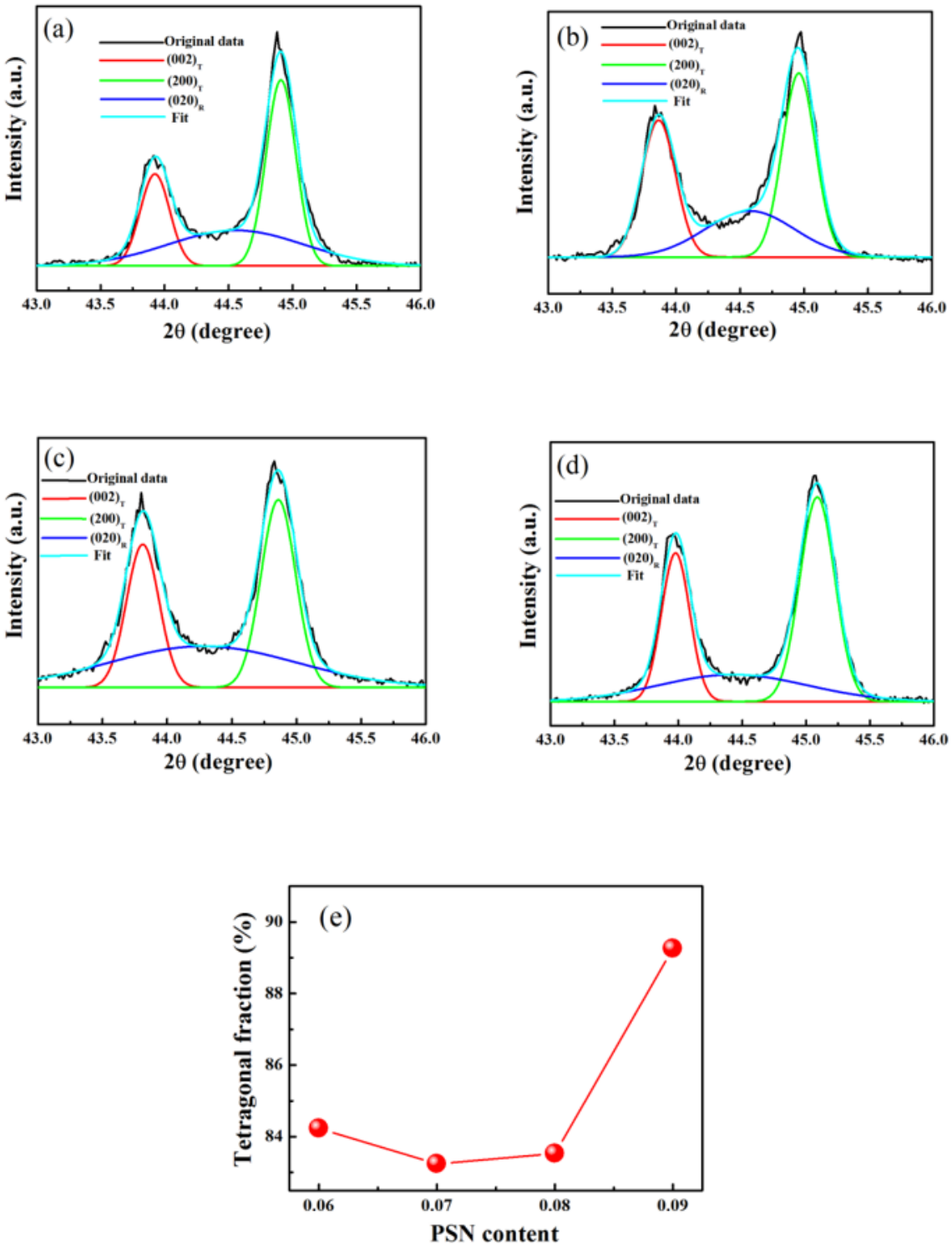

Figure 3

XRD patterns of (200) plane for xPb(Sc1/2Nb1/2)O3-(1-x)Pb(Hf0.47Ti0.53)O3 samples: (a) x=0.06; (b) x=0.07; (c) x=0.08; (d) x=0.09; and (e) volume fraction of tetragonal phase as a function of PSN content.

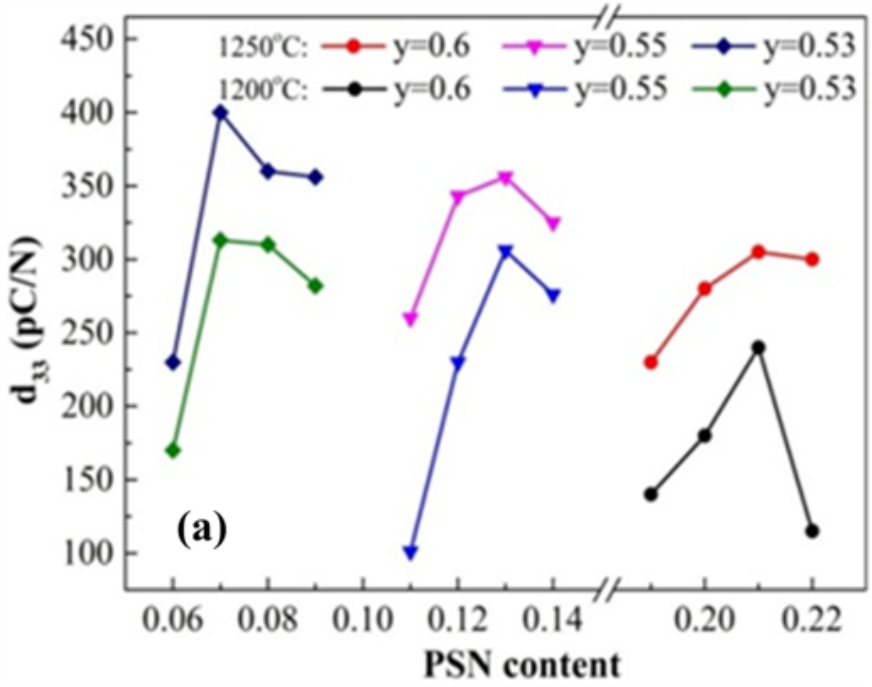

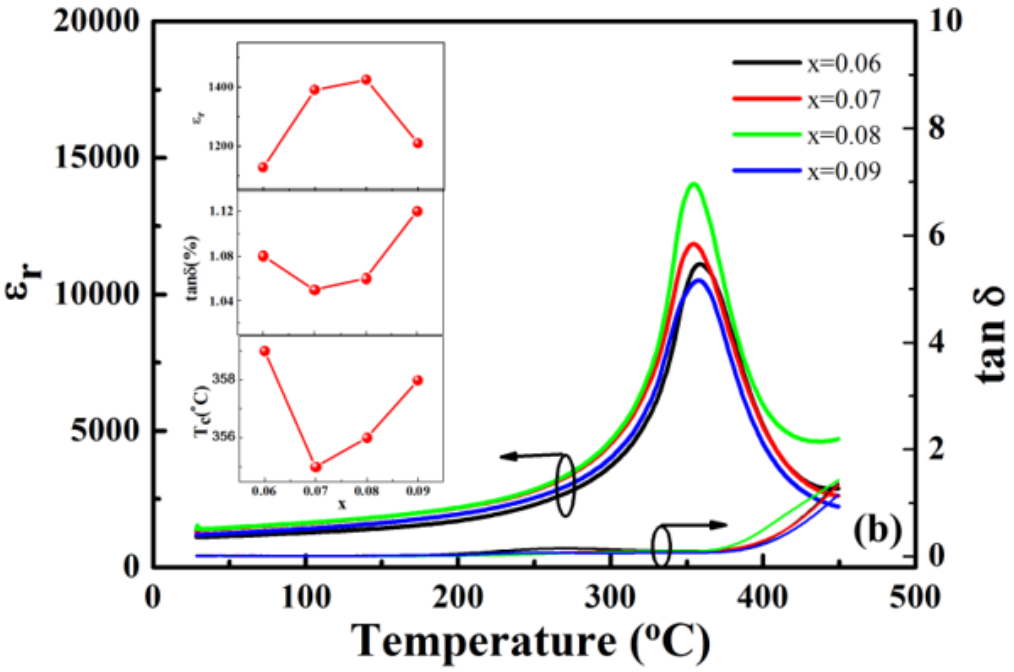

Figure 4

(a) Piezoelectric coefficient d33 of xPb(Sc1/2Nb1/2)O3-(1-x)Pb(Hf1-yTiy)O3 ceramics sintered at 1200 and 1250 °C. (b) Temperature dependence of the relative dielectric permittivity of xPb(Sc1/2Nb1/2)O3- (1-x)Pb(Hf0.47Ti0.53)O3 sample. The inset shows the dielectric parameters and Curie temperature as a function of PSN content.

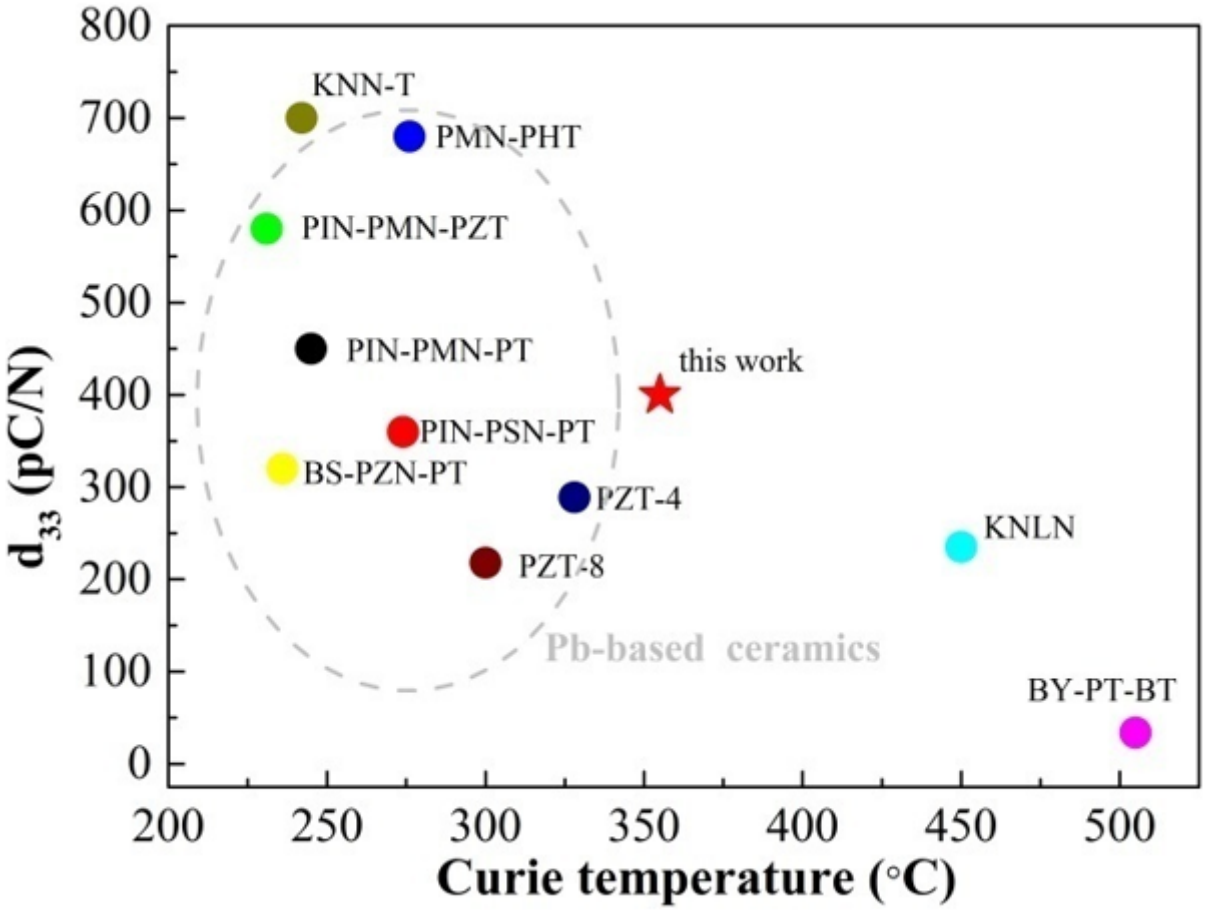

Figure 5

Comparison of Curie temperature and piezoelectric constant of different piezoelectric ceramics.

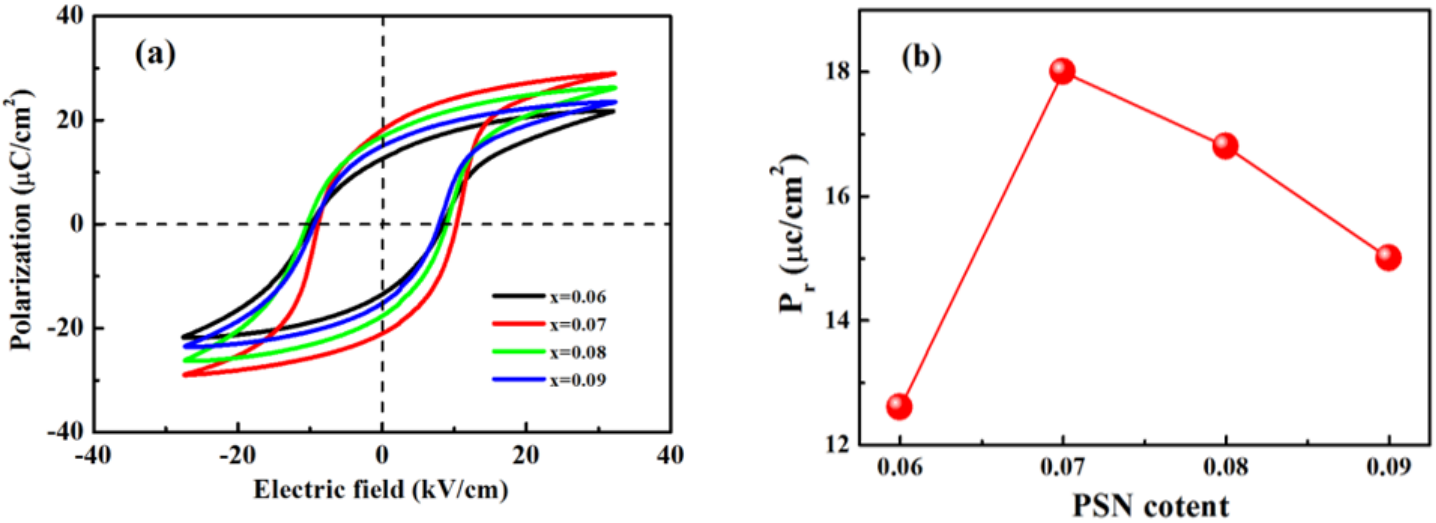

Figure 6

(a) Hysteresis loops for xPb(Sc1/2Nb1/2)O3-(1-x)Pb(Hf0.47Ti0.53)O3 samples at room temperature; (b) Remnant polarization (Pr) as a function of PSN content.

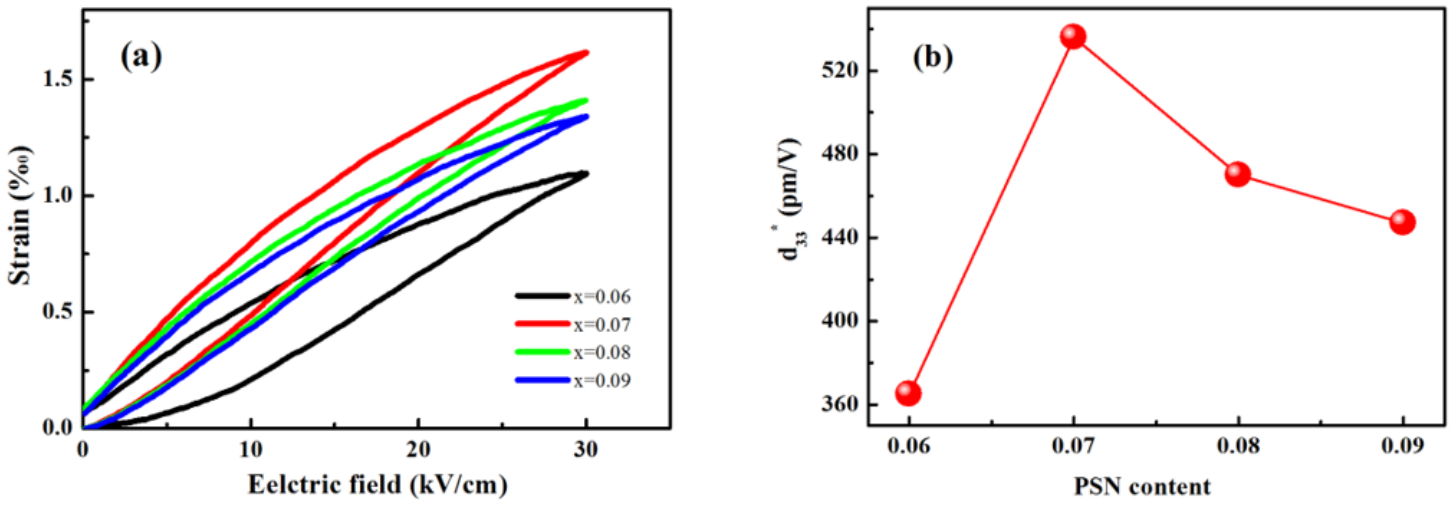

Figure 7

(a) Unipolar strains of xPb(Sc1/2Nb1/2)O3-(1-x)Pb(Hf0.47Ti0.53)O3 samples at room temperature; (b) The d33* as a function of PSN content.

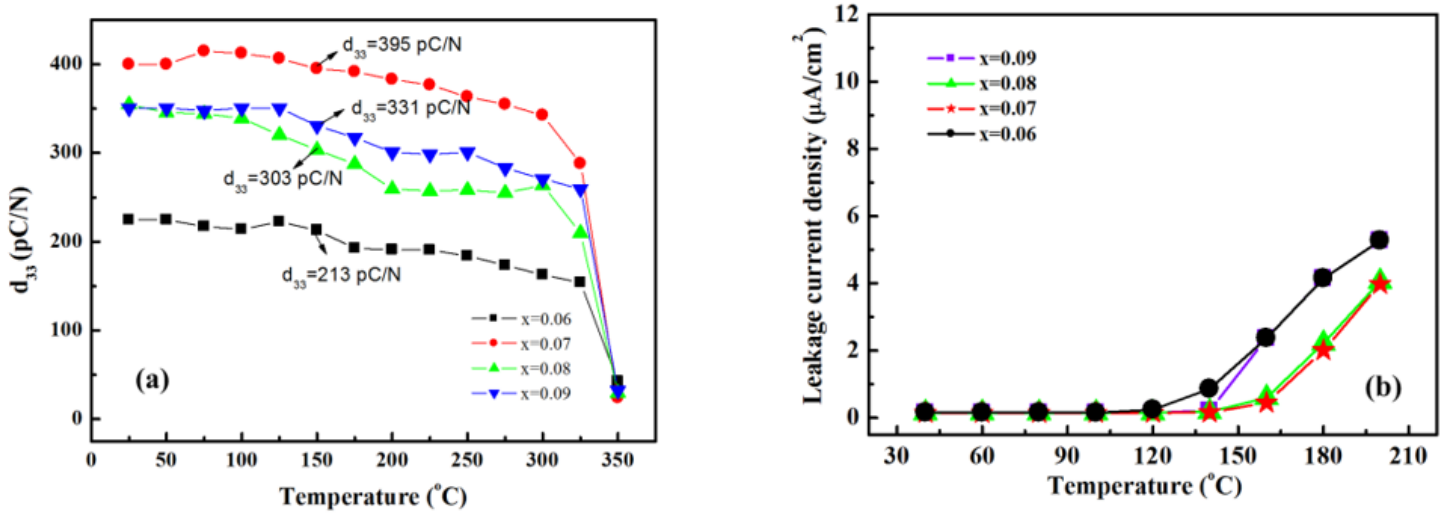

Figure 8

Temperature stability of (a) d33 and (b) leakage current density for xPb(Sc1/2Nb1/2)O3-(1-x)Pb(Hf0.47Ti0.53)O3 samples.

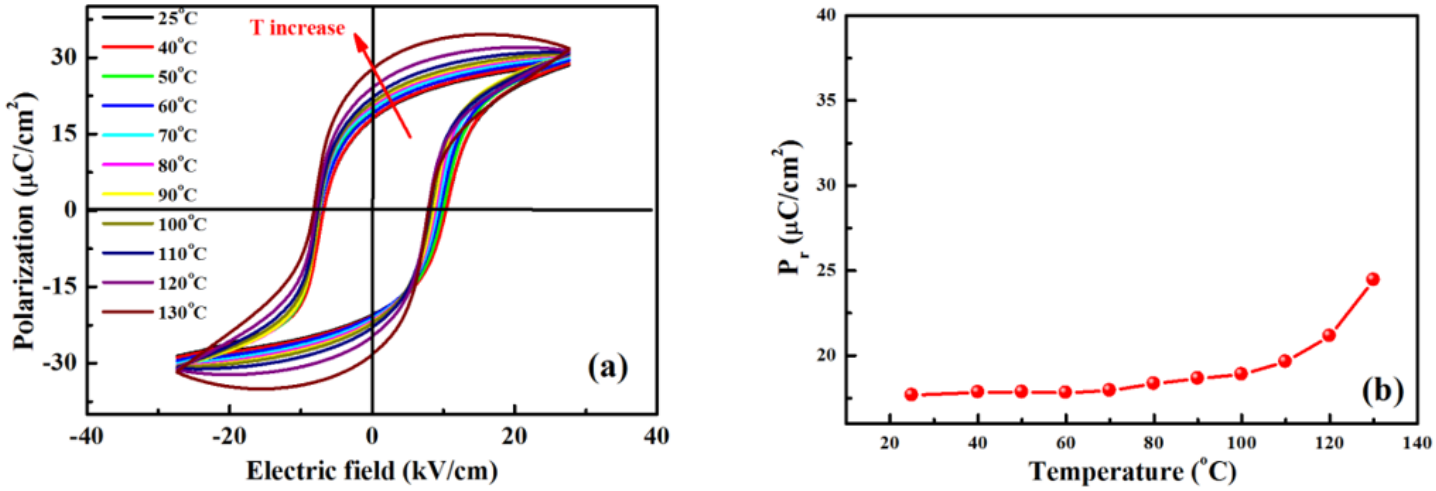

Figure 9

(a) Temperature dependence of P–E loop for 0.07Pb(Sc1/2Nb1/2)O3-0.93 Pb(Hf0.47Ti0.53)O3 sample; (b) Remnant polarization (Pr) as a function of temperature.

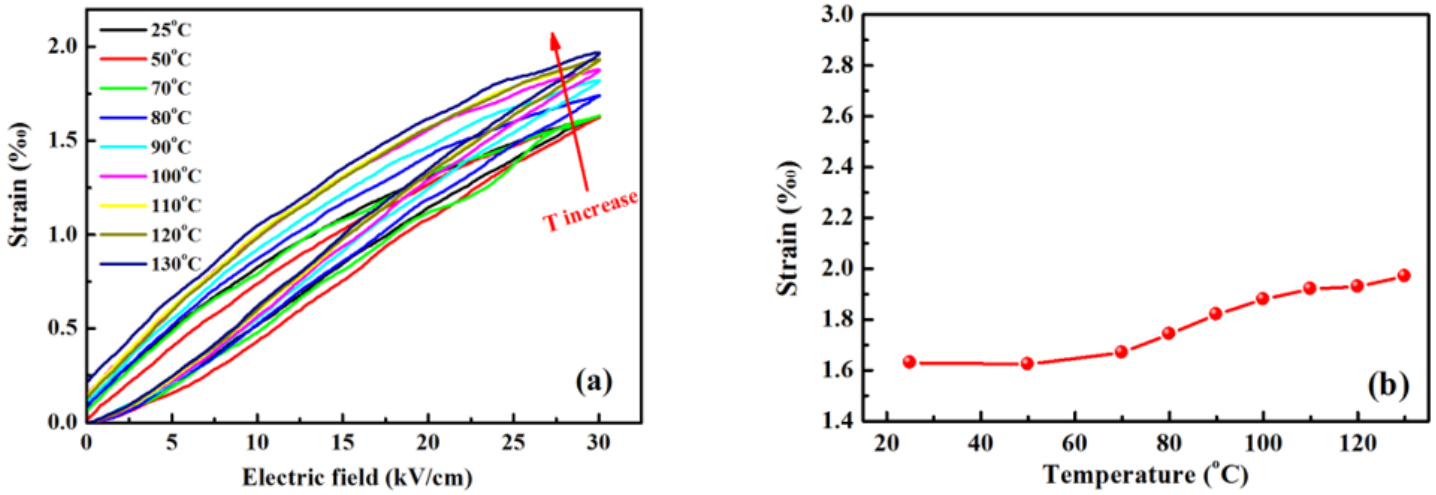

Figure 10

(a) Temperature dependence of unipolar strain for 0.07Pb(Sc1/2Nb1/2)O3-0.93 Pb(Hf0.47Ti0.53)O3 sample; (b) Strain as a function of temperature.